

MODELING AND SIMULATION OF A HEALTH MONITORING SYSTEM IN AN ANALOG MOTOR

T. C. Miller and G. A. Ruderman
Air Force Research Lab
Edwards AFB, CA 93524

ABSTRACT

Finite element modeling of a cross section of a solid rocket motor is used to determine the relationship between several variables in a health monitoring system. The system consists of pressure sensors mounted on the inner case wall. In a pressurized motor, differences among the sensor readings are indicative of crack growth in the propellant. The computational data is used to determine the relationship between sensor sensitivity, the number of sensors, and the minimum detectable crack size. The method of determining the relationships is applicable to other loading conditions, such as thermal loading.

INTRODUCTION

A solid rocket motor is a thick-walled pressure vessel constrained by a relatively rigid outer case material. The constraint of the outer case causes radial and hoop stresses substantially different from those developed in simpler single material thick-walled pressure vessels.¹ One of the important differences is that the hoop stresses for a solid rocket motor are negative. This has a bearing on axial crack formation and development, which depends largely on hoop stresses to provide the driving force for crack propagation. Pressure loads on the faces of the crack also affect the tendency for fracture.² Without the presence of pressure on the crack faces, axial cracks located on the inner bore of solid rocket motors would have difficulty growing.

Engineers are concerned with the presence of cracks in solid rocket motors due to the expense of the motor itself, the payload, the operating and maintenance costs, and the danger inherent in a catastrophic event. Even more benign cracks that don't fully propagate may affect the thrust of the motor, endangering mission success. Because of this, the *Service Life Assessment Technology Project* has sought the cooperation of multiple agencies and nations to study solid rocket motor behavior in many respects, including fracture mechanics.

Ideally, motors could be made from materials that never experienced cracks, but the multi-functional nature of the propellant material makes improving the fracture toughness difficult. Given these limitations, detection of cracks and prediction of their behavior become important. This is not easy either due to many complicated features of the system: materials with low toughness and stiffness, sensitivities to environmental variables such as temperature and humidity, large system size, and long service lives. Detection of cracks in solid rocket motor is important, but must be done in an effective and cost effective manner.

COMPUTATIONAL MODELING OF A HEALTH MONITORING SYSTEM

One part of the solution can be the use of health monitoring systems.^{3,4,5,6,7} In general, this is a method by which real time sensors are used to detect important changes to a structure. In the case discussed here, stress transducers mounted along the inside case wall respond to crack initiation and growth by changing their output. An analog motor (a smaller version of a full scale motor intended for research and experimentation) is to be instrumented with these devices. Loads are applied prior to any crack development to determine baseline values for the sensors. Later crack development will be revealed through changes in sensor readings. The sensors themselves form a health monitoring system, with the number of sensors, their sensitivity, the location and size of the crack, and the type and size of the applied load all affecting the overall system capability. To analyze the proposed system and

determine the relationship between these variables, computational modeling is used. The modeling efforts help determine an acceptable configuration for the monitoring system. Additionally, the method by which these variables are examined is developed. The methodology itself is not motor specific, and can be applied to systems with different loads (for example, the methods developed here work with either pressure loadings or thermally induced loads). The conclusions regarding the monitoring system for the analog motor will be verified later by actual experimental work.

The actual analog motor itself is 21.5 in. (533.4 mm) long, 5 in. (127.0 mm) in diameter, and has a 1.0 in. (25.4 mm) diameter circular inner bore and a case wall with a thickness of 0.25 in. (6.3 mm). The materials comprising the motor include case material, insulator, liner, and propellant. The case material acts at all times as a linear elastic material, but the other materials, though modeled as linear elastic in this study, can have much more complicated material responses. For the modeling work here, only two materials are considered: the case material and the propellant. Both are modeled as linear elastic, and the geometry is a two-dimensional plane strain model of a cross section of the motor. Previous models of this motor indicated that the two-dimensional plane strain model would be an adequate representation.

Figure 1 shows the mesh associated with the finite element analysis. The model uses eight-noded plane strain elements. Due to the incompressible nature of the propellant material, these are hybrid elements, which incorporate pressure variables and prevent problems with global stiffness matrix singularities.⁸ A convergence study was conducted to determine reasonable sizes for the elements. The convergence criteria were specific results for different element sizes: radial and hoop stresses for uncracked pressurized motors and the J integral values for several crack sizes in cracked pressurized vessels. The conclusion reached was that elements with a dimension of 0.050 in. (1.3 mm) in the radial direction were adequate. In the circumferential direction, the disk is broken up into 6° sectors.

As Figure 1 shows, only half of the cylinder is modeled -- the axial crack shown prevents use of a quarter disk, but symmetry does allow a half disk, with field variables on the right half of the cylinder mirrored on the left. The displacement boundary conditions are horizontal constraint of the left faces except for the crack faces and vertical constraint of a single node at the far right. The first condition is required by symmetry considerations, and the last constraint is required to prevent rigid body translation. The applied load was a pressure load of 500 psi (3,447 kPa) on the inner bore of the cylinder. For models incorporating an actual crack, pressure loads were also applied to the crack faces. The model shown in Figure 1 shows a 1.0 inch (25.4 mm) crack, but to obtain complete results, a number of models having different crack sizes were used (0.25, 0.30, 0.35, 0.40, 0.45, 0.50, 0.60, 0.70, 0.80, 0.90, and 1.00 inch cracks were examined)(6.3, 7.6, 8.9, 10.2, 11.4, 12.7, 15.2, 17.8, 20.3, 22.9, and 25.4 mm).

DISCUSSION

The uncracked pressure vessel experiences complete symmetry in the circumferential direction. As discussed previously, due to case constraint the hoop stresses are negative, as are the radial stresses. The hoop stresses are important because they are one of the two driving forces for crack propagation (the other being the pressure loads applied to the crack faces). The radial stresses are important because stress sensors mounted near the inside case wall would sense pressure by actually sensing the radial components of the stress tensor. Figure 2 shows the radial and hoop stresses as a function of radial coordinate in the propellant. Adjacent to the case wall, the elements show a radial stress value of -480 psi (-3,309 kPa) for a pressure load of 500 psi (3,447 kPa).

Figure 2 gives results for an uncracked two-material thick-walled cylinder. The introduction of a crack to the model destroys the symmetry of the model and results, so that plots such as those shown in Figure 2 depend on angular orientation. Both hoop and radial stresses are affected by the presence of a crack. Figure 3a shows plots of the radial stress near the case wall as a function of angular orientation θ (see Figure 3c) for all of the cracked models analyzed here. To obtain this plot, the radial stresses near the case wall are determined by the elements adjacent to the case wall. For these elements, the results at the integration points are interpolated to the centroid of each element, so that each element gives a single value for radial stress. The figures show that the crack acts to relieve the radial stresses, giving minima at approximately 40° from the crack axis, with the location of the minima varying slightly as the crack size changes.

The important measurement here is not really the stress reading on a gage, but the change in the stress reading from a baseline value of -480 psi (-3,309 kPa). The changes in readings are shown in Figure 3b. The sensors used must be precise enough to detect these changes, but must also have a range adequate for the baseline readings in Figure 3a. However, the actual monitoring system is composed of a finite number of sensors, and will not necessarily have a gage positioned at the maxima in Figure 3b, since the site for crack nucleation is not known *a priori*. The analysis of the modeling efforts makes extensive use of Figure 3b to determine the relationship between the variables. To make this problem tractable, the finite element data points (shown in Figure 3b) are fitted with fifth order polynomials (also shown in the Figure 3b) so that a computer program can easily determine the inner case wall radial stress component as a function of θ .

The computer program is easily understandable. Figure 4 shows the ideas behind the program. A certain number of sensors and a certain crack size are assumed for each run of the program. The sensors are all mounted equidistant from each other. The angle between the crack and the sensor is incremented in small amounts, and for any arbitrary orientation, the sensor readings are determined based on the curve fits for the finite element data, and the maximum of these readings is recorded. The maximum reading is important because it must be greater than the sensor sensitivity for detection to be possible. Each time the program is run, a plot of the maximum sensor reading as a function of ψ is produced (ψ is the angle between the crack plane and the first sensor encountered in the clockwise direction). An example of this process is shown for three sensors and $a = 0.45$ in. (11.4 mm) (see Figure 4a). Many sequential runs of the program give a family of curves. Figure 4b shows the curves for the various crack sizes with three sensors. Multiple plots are produced by considering different numbers of sensors.

Figure 4b also shows the relationship between each graph and the required sensitivity of the stress gages. In this figure, a sensor sensitivity of 8 psi (55 kPa) is supposed. This is shown as a horizontal line on the graph. From the figure, it is apparent that cracks having sizes of $a = 0.45$ in. (11.4 mm) or less will not be detected regardless of sensor orientation, and cracks with sizes of 0.70 in. (17.8 mm) or more will be detected regardless of sensor orientation. For cracks with a depth of $a = 0.50$ in. (12.7 mm) or $a = 0.60$ in. (15.2 mm), the crack may or may not be detected, depending on the crack location relative to the sensors, characterized by the angular value ψ . By this same logic, the minimum value for each curve is really the required sensor sensitivity for a given number of sensors and a given crack size. The minimum value of each of these curves can be recorded, giving a table of required sensitivity as a function of the number of sensors and the crack size. This data can be analyzed and conclusions drawn about the requirements for the monitoring system. Figure 5 shows these results in graphical form.

SUMMARY AND CONCLUSIONS

After analysis of the modeling results, we are able to state the following conclusions:

- For a 500 psi (3,447 kPa) pressurization loading condition, the ideal number of sensors to use is either three or four. Some improvement in system sensitivity is gained by going from three to four sensors, but using additional sensors gives negligible gains in performance (this may be different for different loading conditions).
- The ability of the system to detect a crack of a certain size depends on the sensitivity of the sensors themselves. For the loading condition discussed, as the sensitivity of the gages varies from about 2 to 14 psi (13 to 96 kPa), the minimum detectable crack size varies from about 0.25 to 1.0 in. (6.3 to 25.4 mm) (see Figure 5b). The minimum detectable crack size can be compared with the critical crack size, which is determined by comparing modeling results from anticipated service loads with fracture toughness measurements for the propellant.
- Computational modeling data can be used to determine the relationship between important variables that characterize the health monitoring system. These variables are the minimum detectable crack size, the required sensor sensitivity, the loading conditions, and the number of sensors used. Once the computational modeling results are obtained, the procedures here can be used to easily determine the relationship between the variables.

FUTURE WORK

One way to introduce an inner bore crack to a developmental motor would be to apply thermal shock to it. The method of analysis proposed above can be used to determine the optimal monitoring system configuration, and this specific problem could be addressed. As another possible use, the 360° rotation of a large scale motor with an inner bore crack would result in varying sensor readings as the motor was rotated. This data could be analyzed as a nondestructive evaluation technique, and the computational modeling and related analysis of the type developed here could be used to determine the number of sensors and their required sensitivity for such a situation.

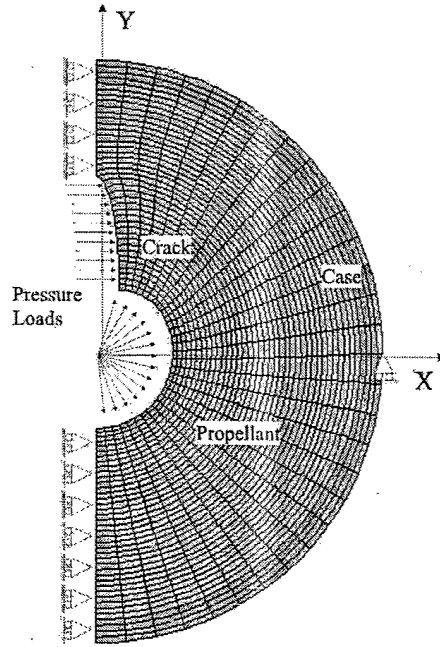


Figure 1 -- Schematic of Mesh, Boundary Conditions, and Loads Used in the Analysis

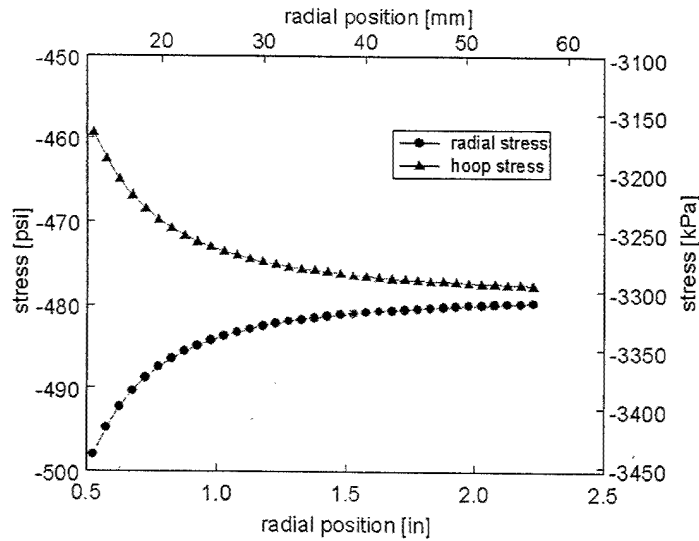


Figure 2 -- Radial and Hoop Stress Results from the Model of the Analog Motor

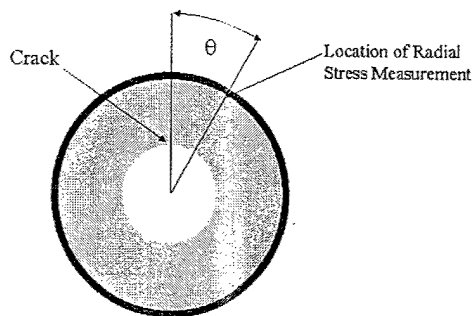
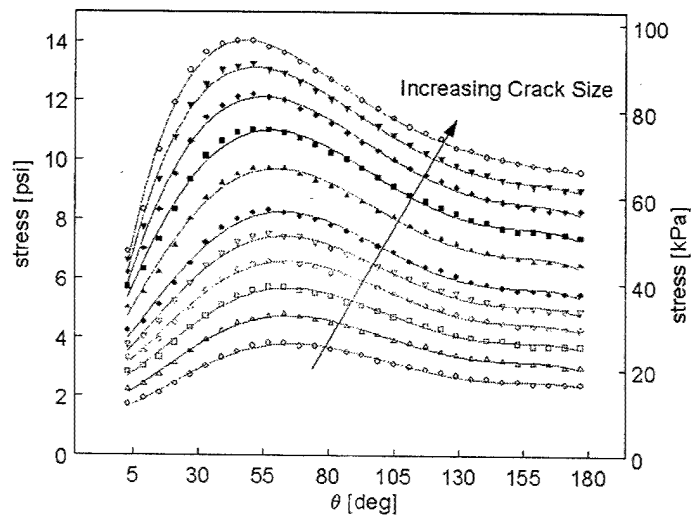
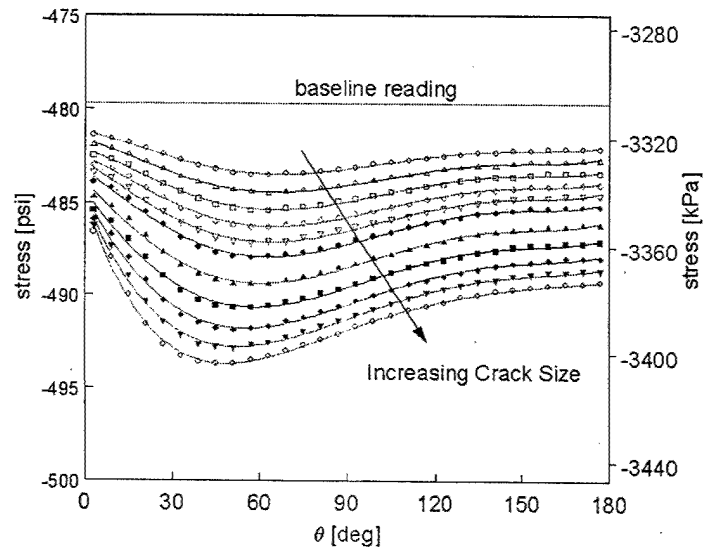


Figure 3 -- Radial Stress Components, Change in Radial Stress Components, and Angular Position Definition

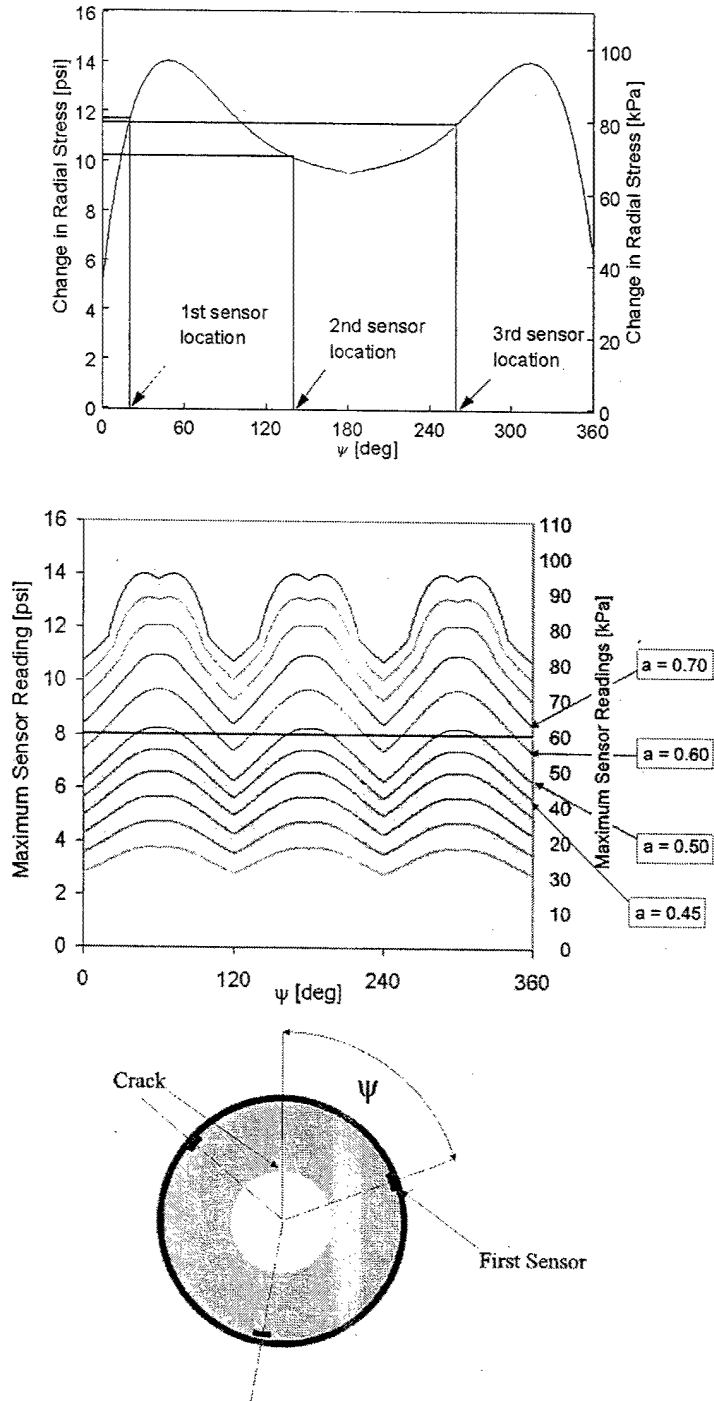


Figure 4 -- Determination of Maximum Sensor Reading from Modeling Data, Maximum Sensor Reading for Three-Sensor System

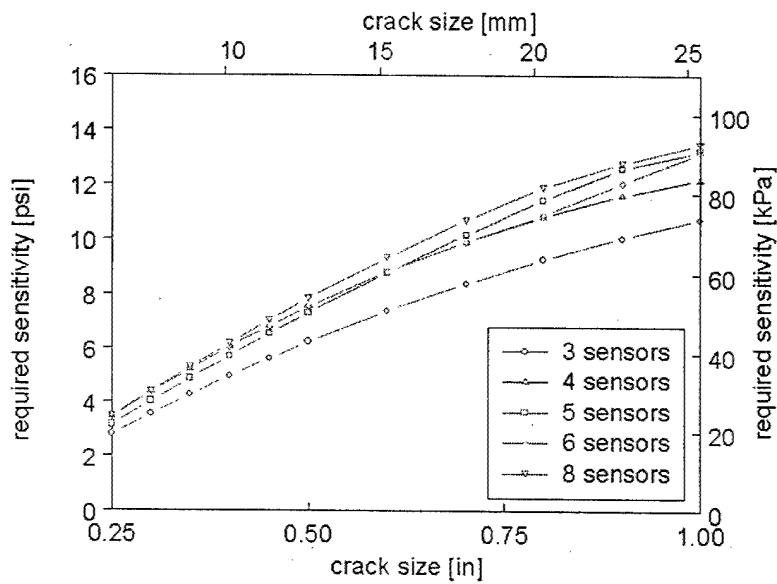
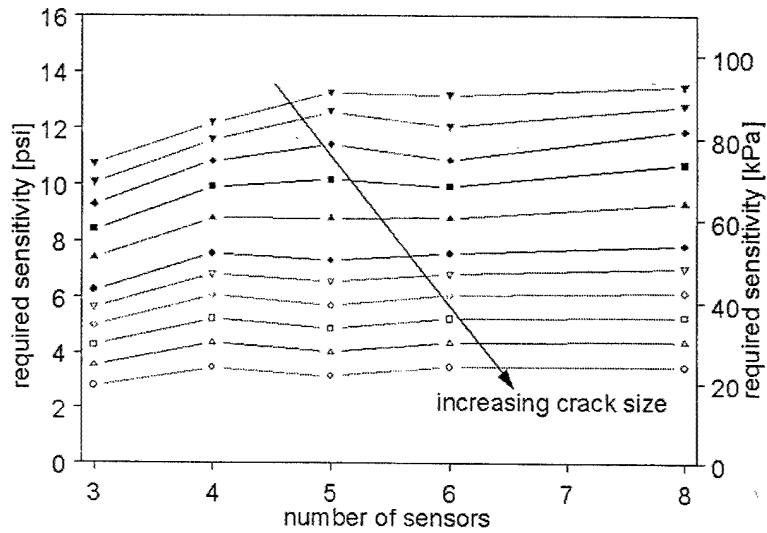


Figure 5 -- Relationship between Sensor Sensitivity, Minimum Detectable Crack Size, and Number of Sensors

REFERENCES:

- ¹ Young, Warren C., Budynas, Richard G., and Roark, Raymond J. *Roark's Formulas for Stress and Strain*. McGraw Hill Professional (2001).
- ² Shannon, R. W. E. and Austin, B. A. The Application of Fracture Mechanics to Failure of Thick-Walled Cylinders. *Instn Mech Engrs*, Vol. C32, 109-118 (1971).
- ³ Chelner, Herbert. *Embedded Sensor Technology for Solid Rocket Motor Health Monitoring*. Interim Report for Phase I SBIR Topic A01-166., Micron Instruments, Simi Valley, California (May 2002).

⁴ Bond, L. J. Inspection of Solid Rocket Motors and Munitions Using Ultrasonics. In *50th JANNAF Propulsion Meeting*, Salt Lake City, Utah, July 2001, pp. 425-460.

⁵ Welle, R. P. Health Monitoring for Graphite/Epoxy Motor Cases. Tech. Rep., Aerospace Corporation, El Segundo, California (May 2000).

⁶ Osborn, J., Brown, B., Amimoto, S., and Fournier, E. Full-scale Delta GEM MPS Demonstration – May 11-12, 1999, Air Force Research Laboratory. Tech. Rep., Aerospace Corporation, El Segundo, California (November 1999).

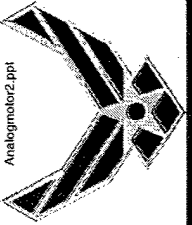
⁷ Osborn, J., Chan, Y. C., Klimcak, C. M., Brown, B., and Williams, B. Graphite-Epoxy Motor Casing Health Monitoring System Demonstration. Tech. Rep., Aerospace Corporation, El Segundo, California (June 1999).

⁸ Hibbit, Karlsson and Sorenson, Inc., 1080 Main Street, Pawtucket, Rhode Island. Abaqus Theory Manual, Version 5.8, Section 3.2.3 Hybrid Incompressible Solid Element Formulation (1998).

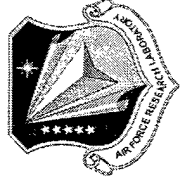
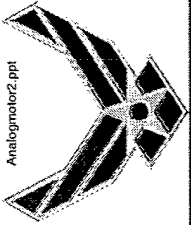
Modeling And Simulation Of A Health Monitoring System In An Analog Motor



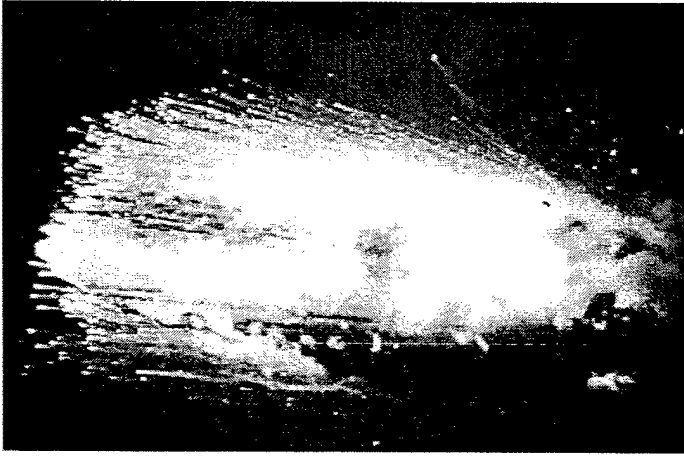
T. C. Miller
G. A. Ruderman
Air Force Research Lab
Edwards AFB, CA



Introduction

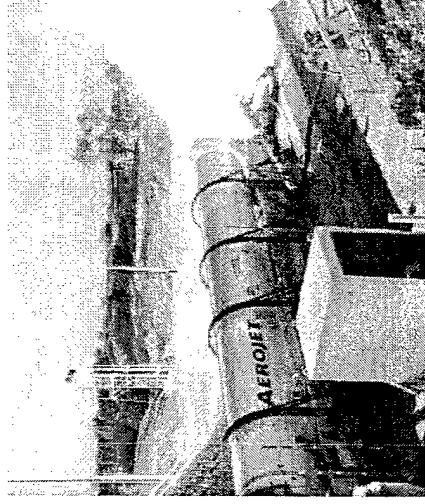


Motivation



Consequences of Failure

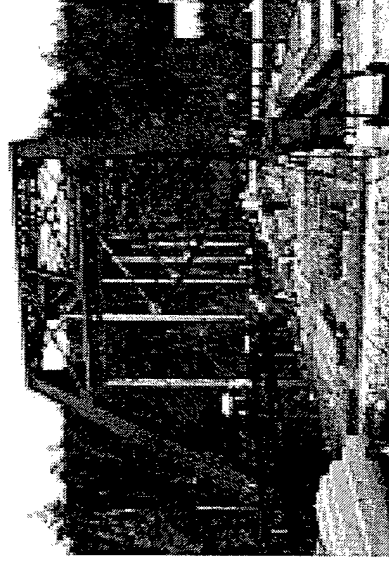
Ways to Ensure Reliability



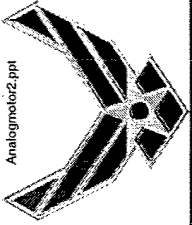
Live Testing



Nondestructive Evaluation



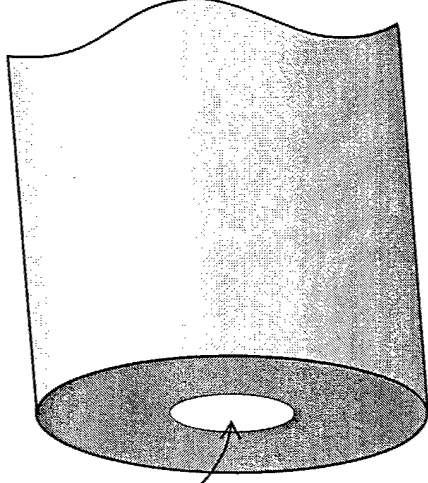
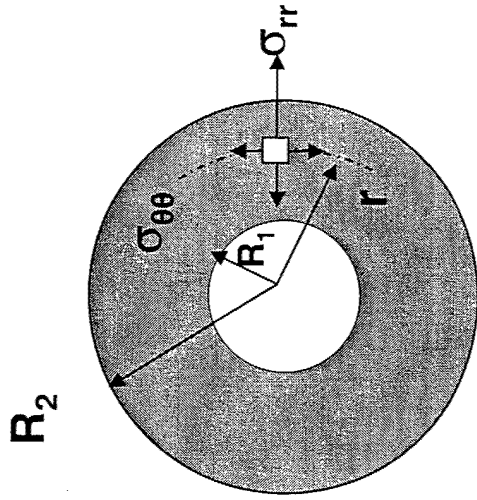
Health Monitoring



Conventional Analysis For Hoop And Radial Stress

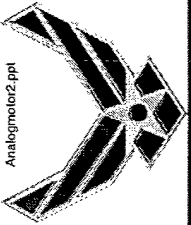


Pressure "P"



$$\sigma_{\theta\theta} = \frac{pR_1^2(R_2^2 + r^2)}{r^2(R_2^2 - R_1^2)} \quad \sigma_{rr} = \frac{-pR_1^2(R_2^2 - r^2)}{r^2(R_2^2 - R_1^2)}$$

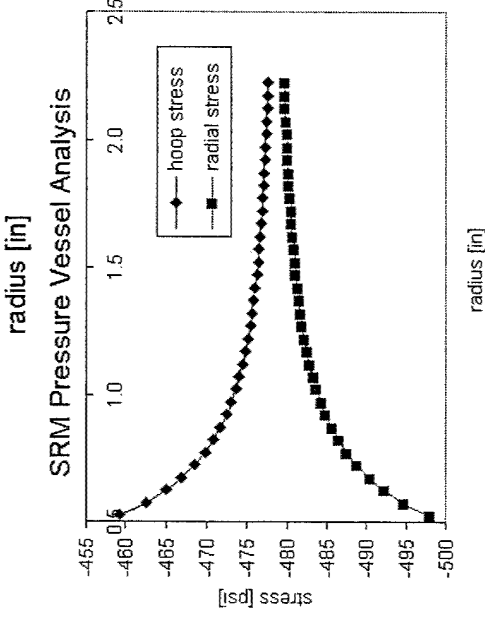
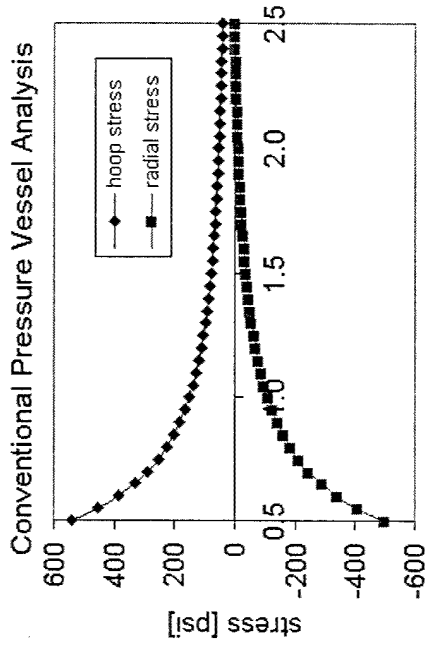
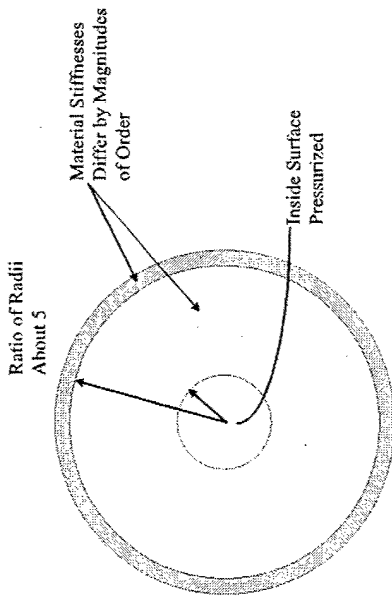
Conventional analysis for thick walled pressure vessels gives tensile hoop stresses but does not apply to solid rocket motors.



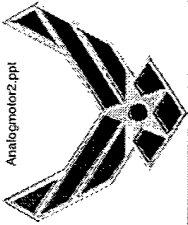
Pressure Vessels And Solid Rocket Motors



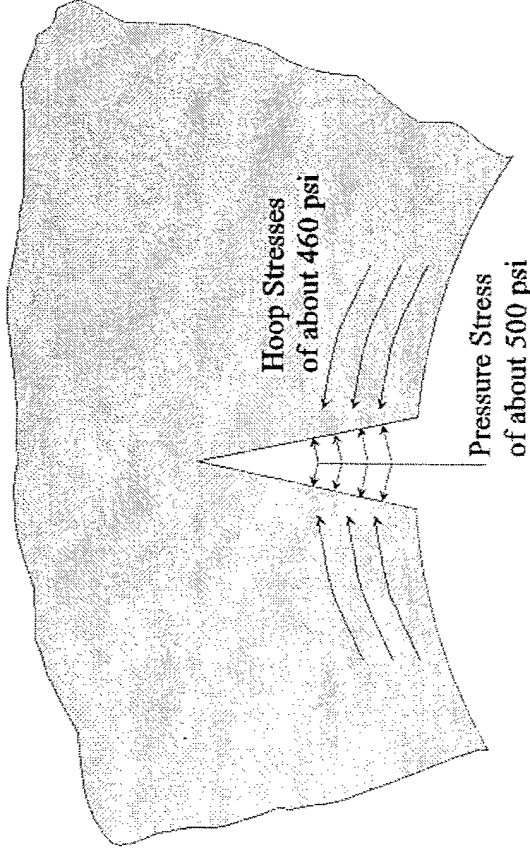
- SRM is thick walled pressure vessel with rigid outer constraint
- Different behavior than for conventional mechanics of materials analysis
- Pressure loads required to open crack



Negative hoop stresses would close the crack if it weren't for the pressure loads on the crack faces.



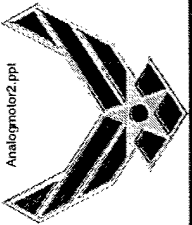
Competing Hoop And Pressure Stresses



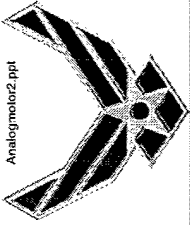
$$K_I = (\sigma_{\theta\theta} + p) \sqrt{\pi a} f \left(\frac{a}{t} \right)$$

Relatively Weak Driving Force

Combination of negative hoop stress and pressurized crack faces results in substantially weaker “driving force” for fracture.

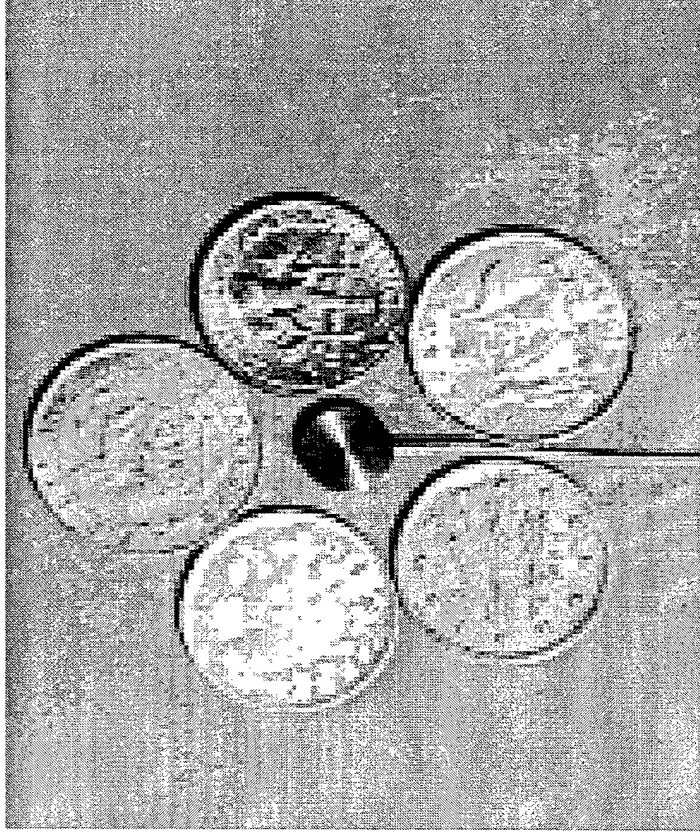


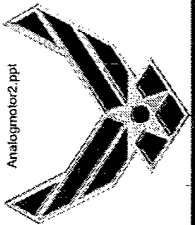
Computational Modeling Of A Health Monitoring System



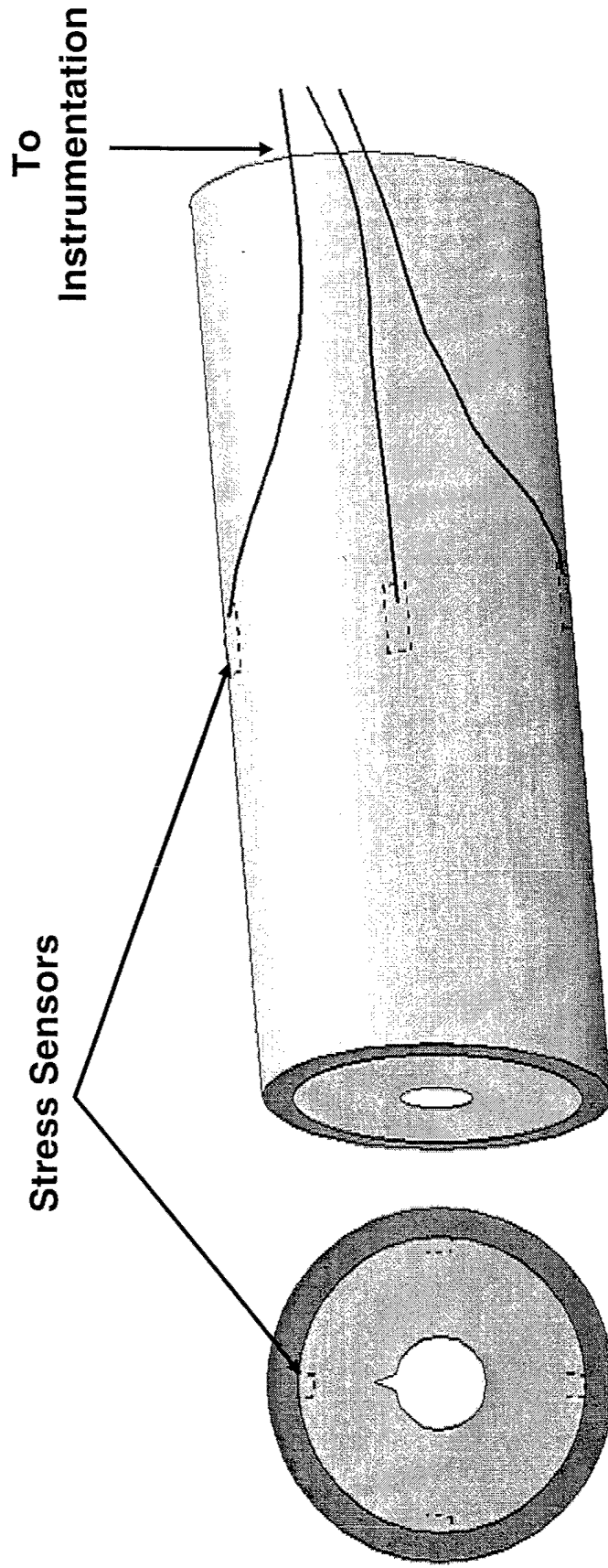
Health Monitoring Systems

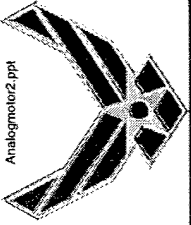
- **General Use**
 - Installed during or after manufacture. System stays with product, makes physical measurements that are indicators of damage (AE, strain, etc.)
- **Use in the Analog Motor**
 - Physical measurement correlates with radial stresses near inside case wall, should be an indicator of inner bore crack growth. For research purposes, crack could be intentionally introduced



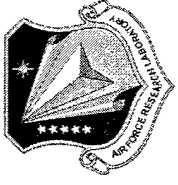


Sensors On Inner Case Wall



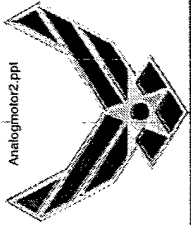


Parameters Affecting HMS Design



- Type and size of load
- Expected crack geometry
- Requirement for minimum detectable crack size
- Number of sensors
- Required sensor sensitivity

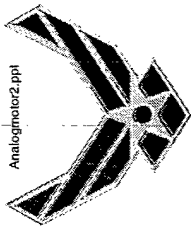
Time constraints prevent considering all of the effects. The relationship between some of the effects can be found.



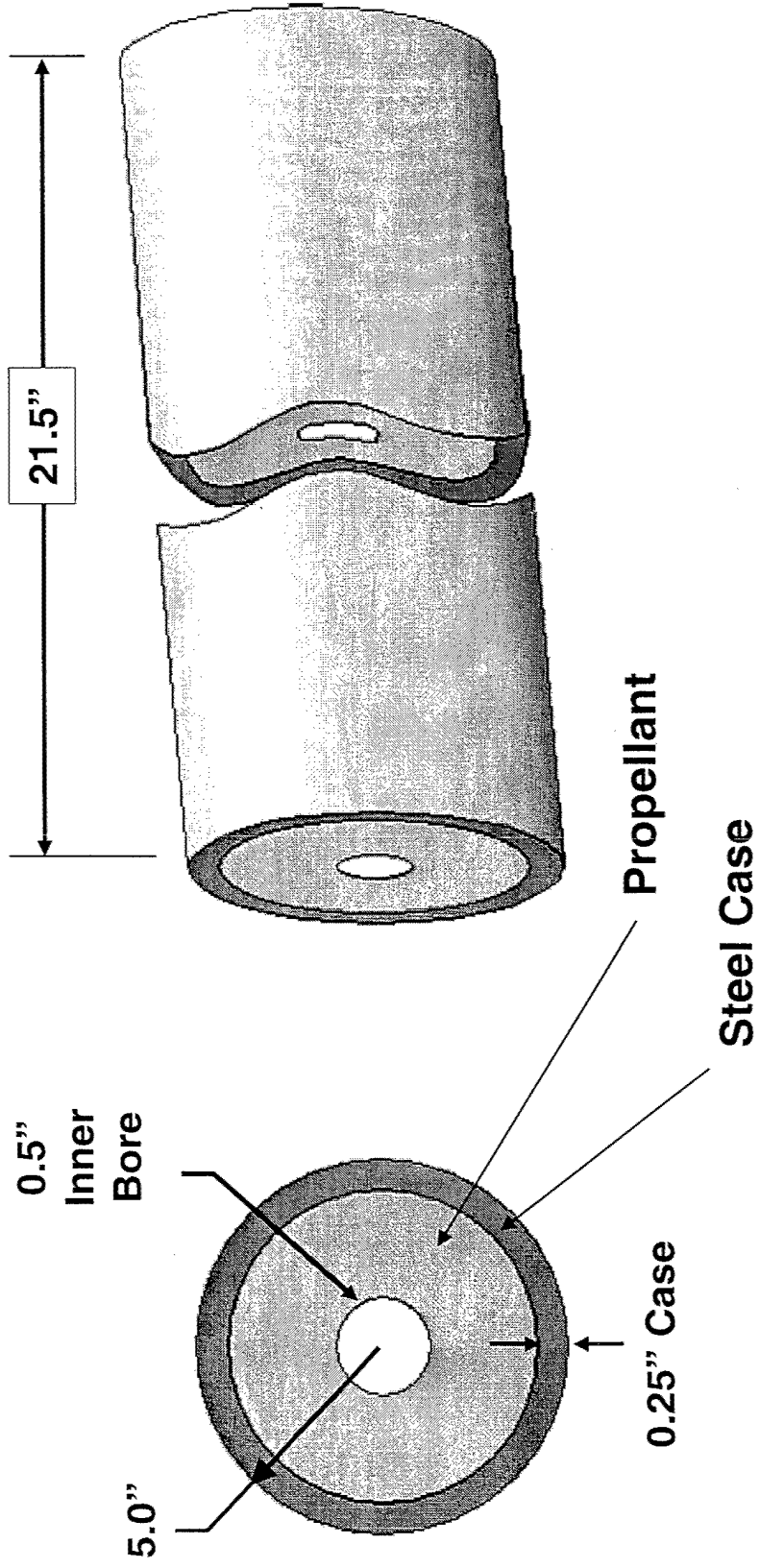
Using FEA As A Design Tool

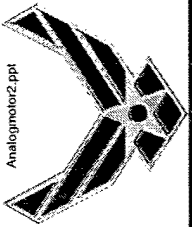
- **General method is developed (can be applied to other situations, e.g., thermal loading)**
- **Specific relationship between variables is found**

This method of analyzing FEA data can be applied to any motor if the loading and crack geometry are prescribed.



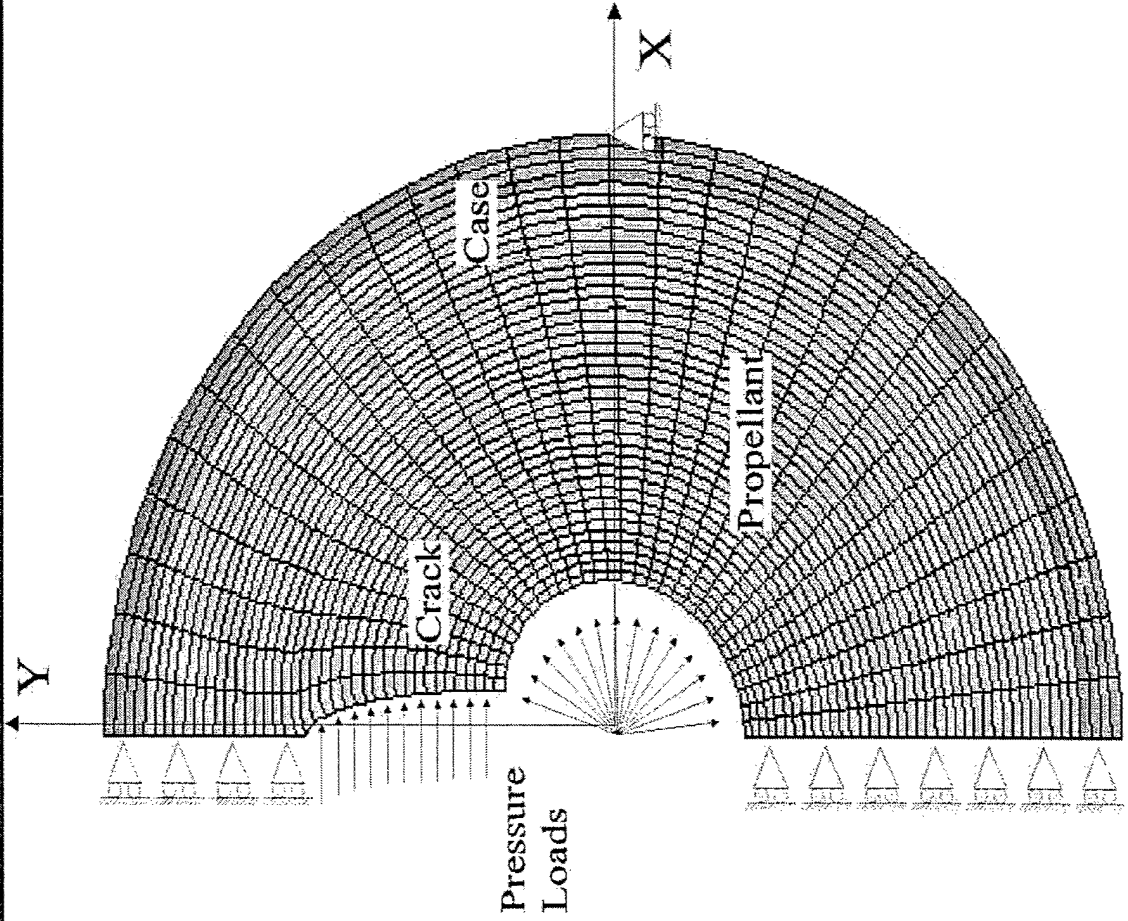
Motor Geometry

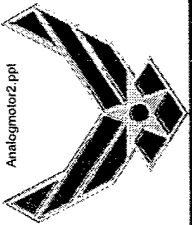




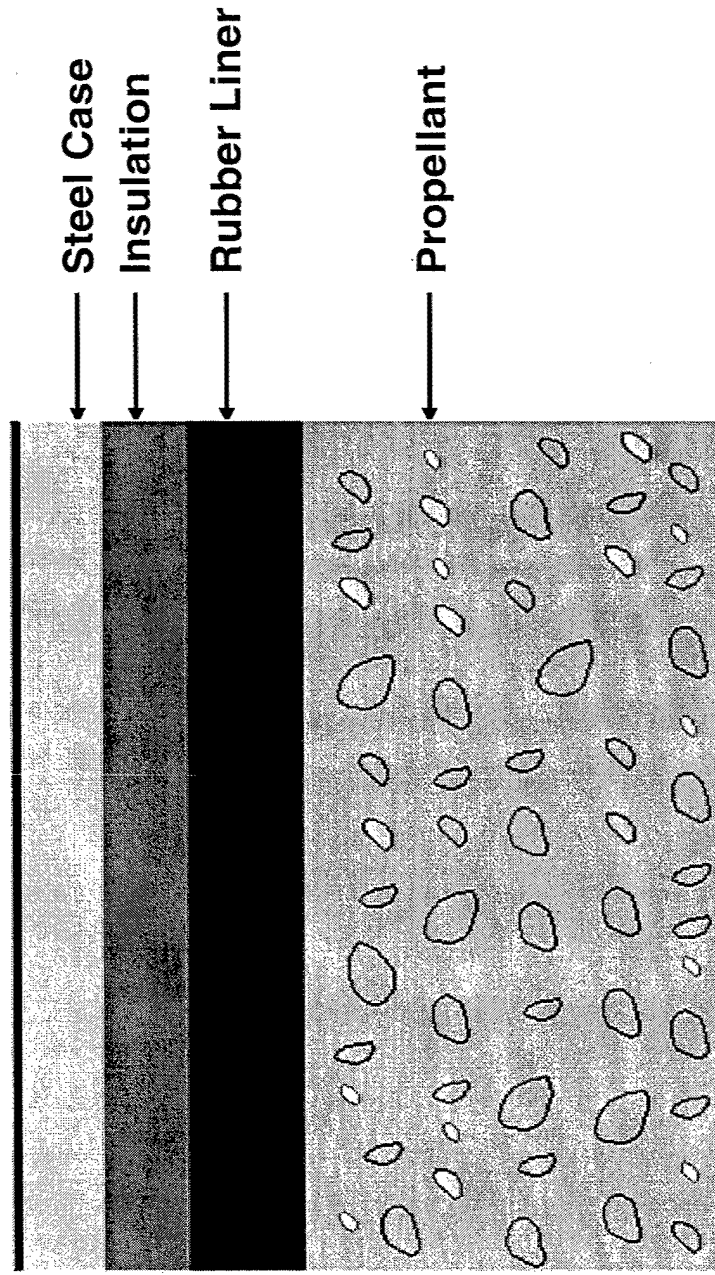
Analogmotor2.ppt

Model Description – Geometry And Loads

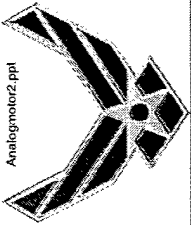




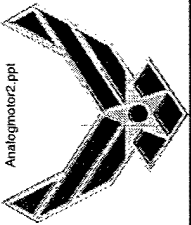
Materials Involved And Simplifications



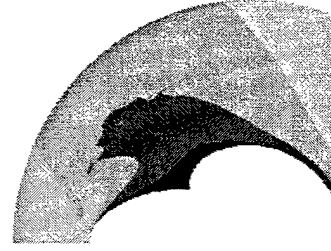
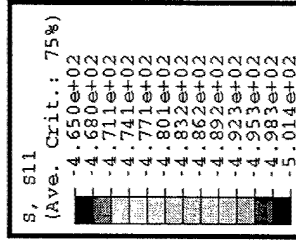
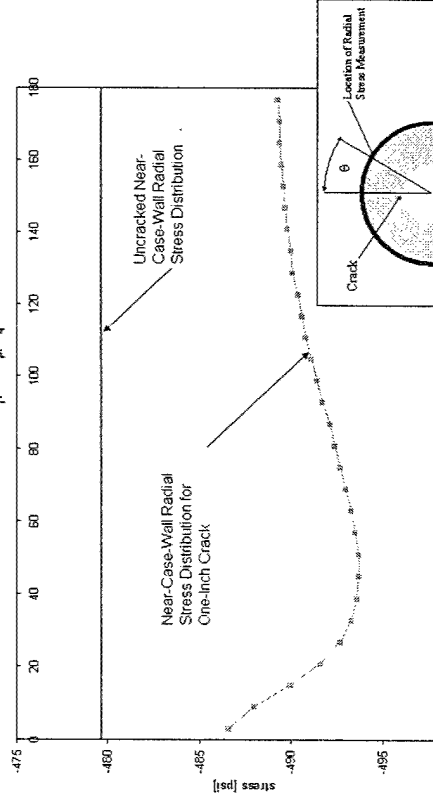
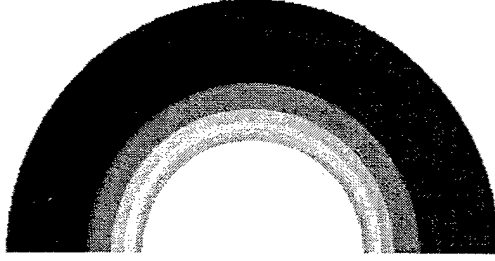
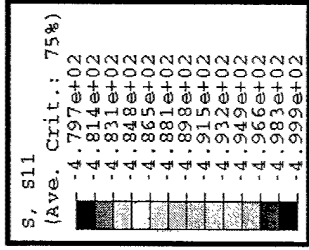
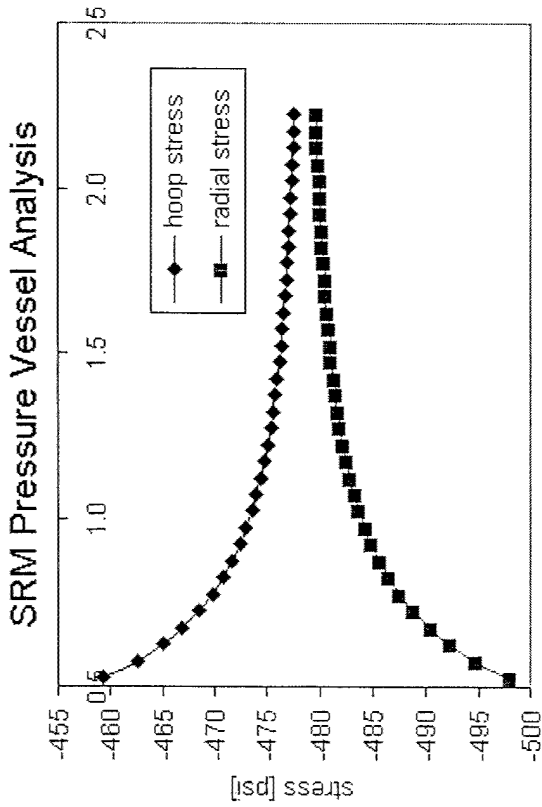
Actual SRM is more complex, but only two materials are used here.



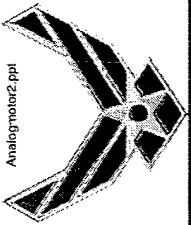
Discussion



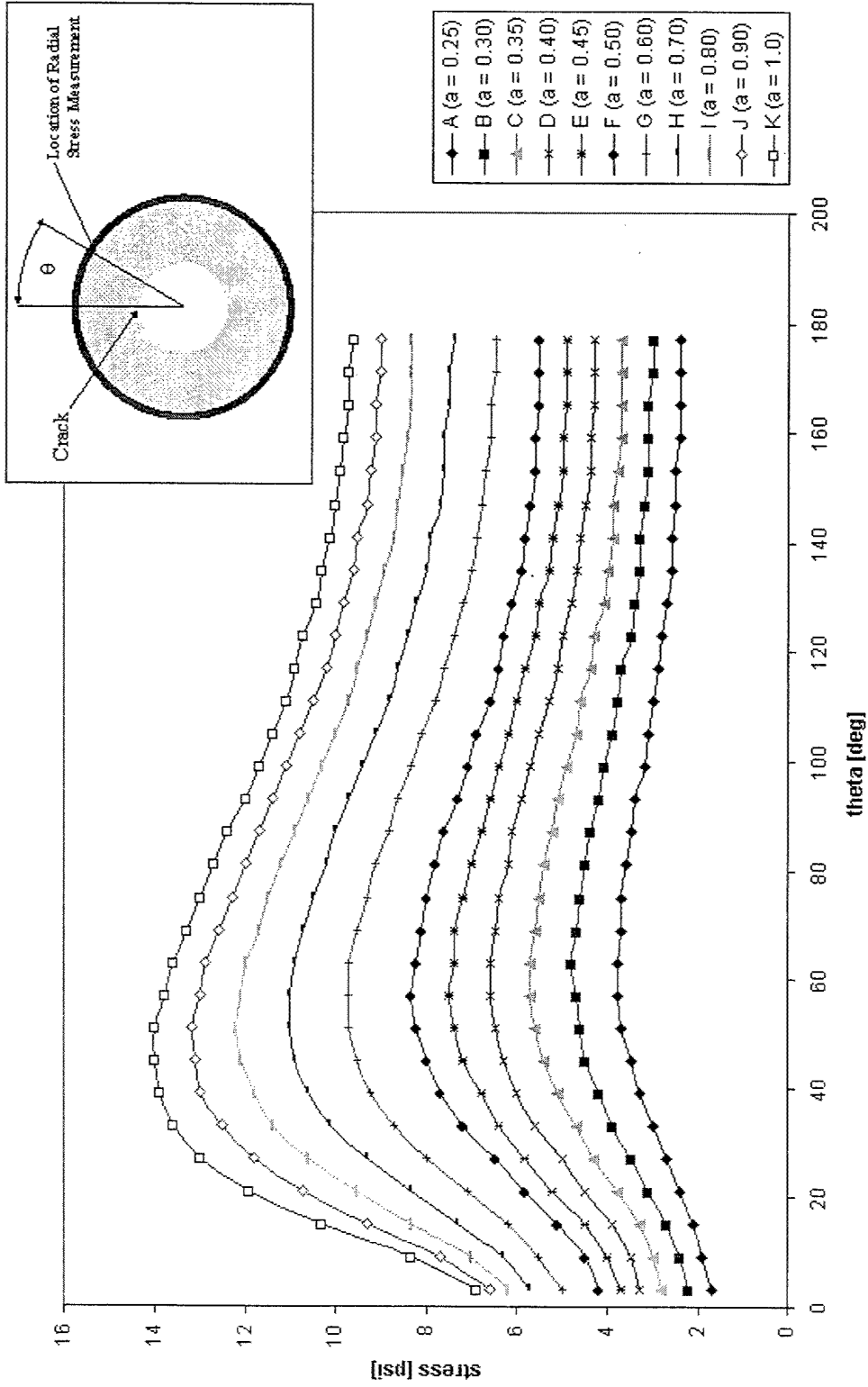
Cracked And Uncracked Solid Rocket Motors



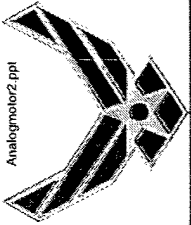
Uncracked motor has "baseline stresses" but presence of crack causes deviations that vary with orientation.



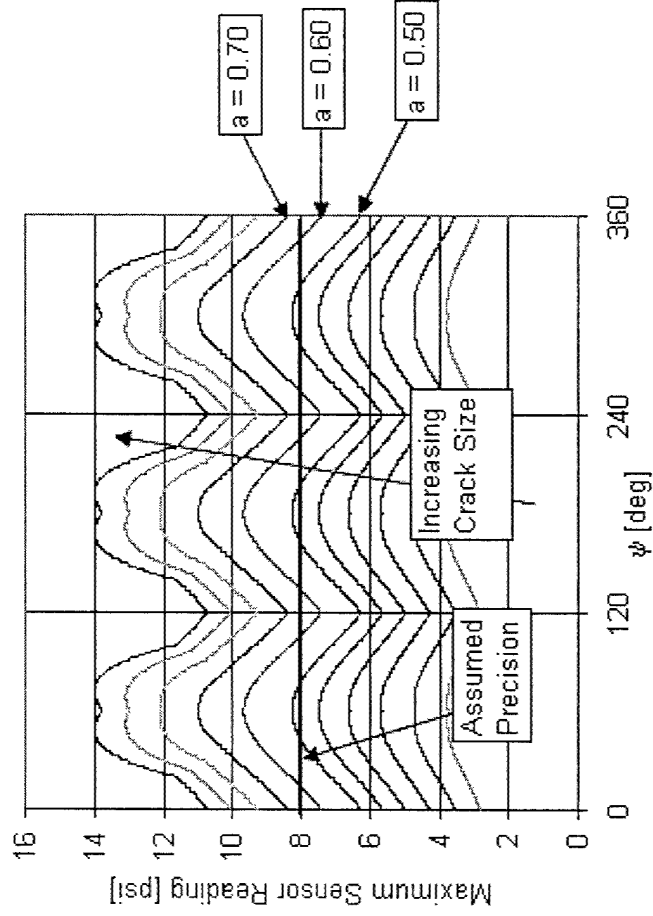
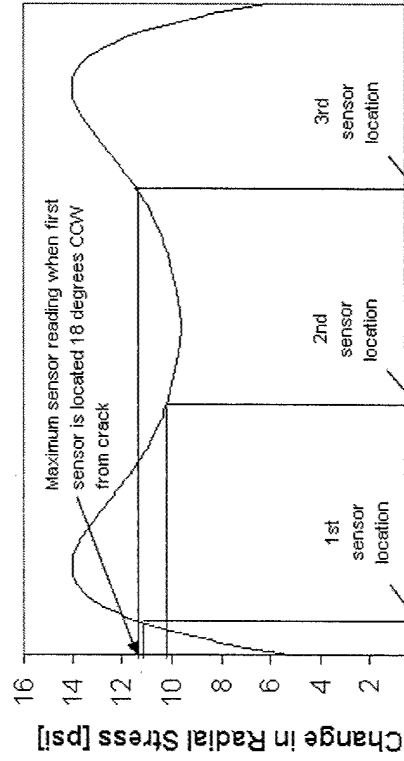
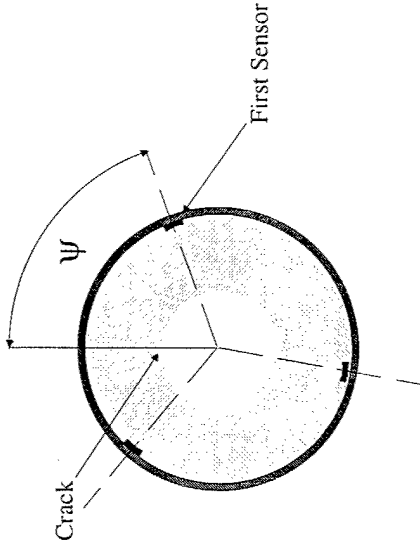
Change In Stresses Near Case Wall Is Felt By Sensors



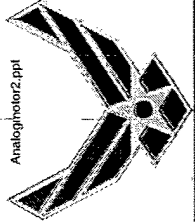
The difference between the “baseline stresses” and the case wall stresses in cracked motor may or may not be detectable.



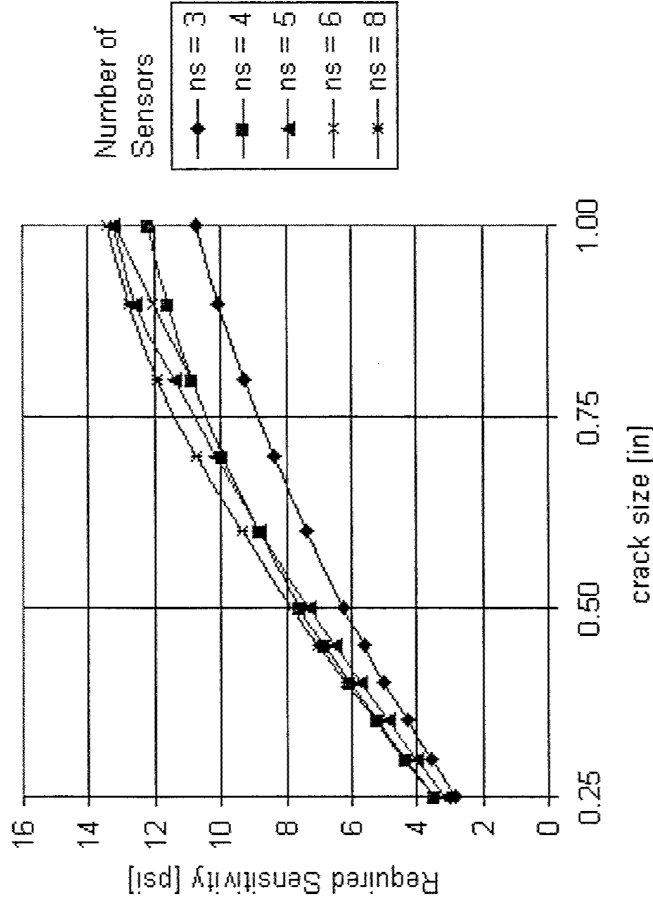
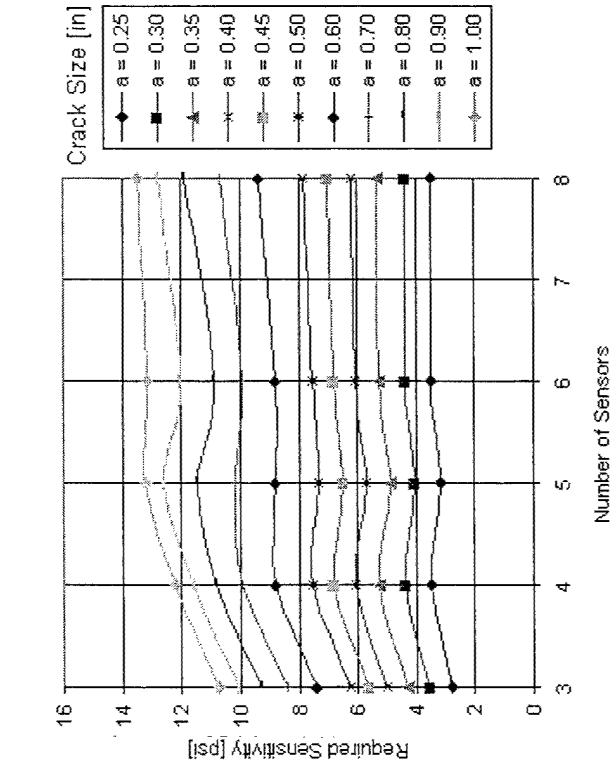
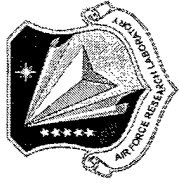
How FEA Results Are Analyzed



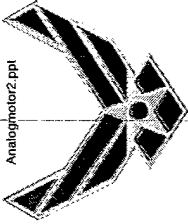
In the worst case scenario, the sensors will be aligned so that the maximum of the three sensor readings will be at a minimum. Detection of the crack may or may not be possible.



Results Relating Number Of Sensors, Sensor Precision, And Minimum Detectable Crack Size



The number of sensors recommended is four (chart on left) and the sensor sensitivity required depends on the crack size (quantified by chart on right).



Summary



- For 500 psi load, use 3 or 4 sensors
- Detection capability depends on sensor precision (this is quantifiable)
- FEA can be used as design tool for health monitoring systems (in general, and specifically for pressure sensors and the analog motor)